Engineering Structures 316 (2024) 118600

Contents lists available at ScienceDirect

Engineering Structures

journal homepage: www.elsevier.com/locate/engstruct

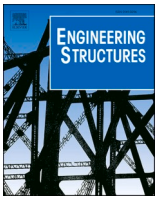

Physics-based flood vulnerability assessment for steel portal framed industrial buildings

Hao Qin [a,*], Matthew S. Mason [b], Mark G. Stewart [a]

[a] School of Civil and Environmental Engineering, University of Technology Sydney, Australia
[b] School of Civil Engineering, The University of Queensland, Brisbane, Australia

ARTICLE INFO

Keywords:
Physics-based flood vulnerability
Hydrostatic and hydrodynamic loads
Industrial buildings
Steel portal frame
Building envelope
Monte Carlo simulation

ABSTRACT

Steel portal framed industrial buildings have been widely used as warehouses, supermarkets, manufacturing workshops and storage facilities around the world. As such, these buildings make up a significant portion of the building stock. Despite this, there remains a lack of the physics-based flood vulnerability models necessary for undertaking detailed community flood risk management activities (e.g., quantitative risk assessment, cost-benefit analysis of risk reduction and resilience enhancement measures at the building level). To this end, this study developed a physics-based vulnerability assessment method for steel portal framed industrial buildings subjected to hydrostatic and hydrodynamic flood actions. Physical damage induced by flood forces to the building envelope (wall siding and fenestration) and the structural framing (steel portal frames and end wall frames) was considered. Monte Carlo simulations incorporate various flood load cases, probability models of demands and capacities as well as major failure mechanisms of different structural and non-structural components to conduct the damage assessment. The flood vulnerabilities for a prototype industrial building link the physical damage of individual building subassemblies to monetary loss ratios considering various inundation depths, flow velocities and flow directions.

1. Introduction

Flood hazards, including pluvial, fluvial and coastal floods, are among the most dangerous and costliest natural disasters worldwide [37]. A significant portion of disaster-induced economic losses and deaths are attributed to flood hazards (Johnson et al., 2016). With the frequency and magnitude of extreme environmental events increasing in some parts of the world under climate change [24], the catastrophic impacts of flood hazards may be exacerbated in the future. Flood-induced damage and losses can be devastating for buildings and infrastructure systems in urban communities. As an example, the recent 2022 flooding in Southeast Queensland and Northern New South Wales caused over AUD$5 billion in building and infrastructure losses [17]. Over AUD$1 billion of these losses were from damage to commercial and industrial buildings [17]. Given such impacts, it is imperative that more is done to manage flood risks and to enhance resilience of the built environment in flood prone areas.

Flood vulnerability for buildings quantifies the extent of physical damage and monetary losses as a function of flood intensity, typically taken as the inundation depth and/or flow velocity. Understanding the vulnerability of different types of buildings is key to estimating losses, reducing risks and improving the resilience of urban communities susceptible to flood hazards. The methods for flood damage assessment are typically either empirical (e.g., [13,48,45]) or physics-based (e.g., [10,27]). Empirical methods utilise observed building damage or loss data from post-disaster surveys and insurance claims, so can be highly specific to a given historical event, site or built environment, and hence may have limited transferability to future events. Purely empirical methods can also have high levels of uncertainty due to limited availability of damage/loss data and the subjectivity and variation of assessors in collecting and interpreting damage/loss data. In contrast, physics-based methods utilize detailed analysis of structural loading, resistance, failure mechanism and performance of the modelled building, which provide a transparent damage prediction at the building component level with explicit physical meanings. This enables cost-benefit evaluation of risk reduction measures (e.g., design enhancement, building retrofit and flood proof) and quantitative resilience assessment (e.g., quantification of functionality loss and recovery process) for individual buildings. These models can also be applied at a community or city scale for a portfolio of buildings with a suite of models required for various

* Corresponding author.
E-mail address: hao.qin@uon.edu.au (H. Qin).

https://doi.org/10.1016/j.engstruct.2024.118600
Received 7 July 2023; Received in revised form 10 June 2024; Accepted 10 July 2024
Available online 20 July 2024

structure types.

Steel portal framed industrial buildings have been widely used in many parts of the world as warehouses, supermarkets, manufacturing workshops and storage facilities, with these buildings making up a large portion of the building stock in many communities and cities. To date, physics-based flood vulnerability models have mostly been developed for brick or masonry residential buildings (e.g., [22]; De Risi et al., 2013; [8,19,11]) and timber framed houses (e.g., [6,2,10,29]) with only vulnerability functions based on empirical data and expert judgement available for industrial buildings (e.g., USACE 2006; [13]). Further, existing vulnerability functions for industrial buildings often relate building damage only to inundation depth with the effect of hydrodynamic actions not considered. Compared to residential buildings, industrial buildings have different flood damage mechanisms, flood load effects and building component resistances that require a new physics-based vulnerability model for this type of structure.

This study describes the development of a physics-based vulnerability model enabling damage and loss assessment for steel portal framed industrial buildings subjected to hydrostatic and hydrodynamic flood actions. The model accounts for physical flood damage to both the building envelope (wall siding and fenestrations) and the structural framing (portal frames and end wall frames). Interior damage due to water inundating is also considered but a more simplified stage-depth damage approach is adopted to estimate these losses. The physical damage assessment is conducted for a prototype industrial building through Monte Carlo simulation considering various flood load cases and critical failure modes of building components. An assembly-based vulnerability method is then used to convert physical damage ratios of individual building subassemblies into monetary building loss ratio for various inundation depths, flow velocities and flow directions. The developed vulnerability model can be used to support flood risk management and resilience enhancement for industrial buildings.

2. Prototype industrial building

The physical damage and monetary losses are assessed for a prototype industrial building with the plan view and structural framing layout depicted in Fig. 1 and Fig. 2, respectively. The building is the same as detailed in Qin et al. [35], with the reader directed to this reference for further detail on the design of this building. The size and structural configuration of the prototype building are representative of mid-to-large sized industrial buildings in Australia. In short thought, the design actions considered for the prototype building are dead load, roof live load, wind load and the corresponding load combinations. Design for flood actions is not specified in the Australian design loading standard (AS/NZS 1170). However, the national construction code [15,20,28,3,38,39,4,40–42,46,9] requires certain types of high-importance building (e.g., hotels, health-care structures) in areas prone to flooding to be designed and constructed to resist floatation, collapse and permanent movement. This is not generally a requirement for industrial buildings due to their lower importance level and therefore flood actions are not considered in the design of the prototype industrial building. The building subassemblies susceptible to flood damage consist of both non-structural (building envelope including wall siding and fenestration) and structural components (steel frame members, roof struts, roof and wall bracing, and column base connections). Table 1 summarizes the design specifications for critical building components considered in the flood damage assessment.

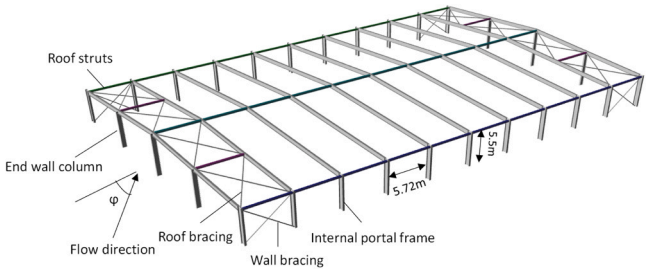

Fig. 2. Steel frame and bracing systems.

3. Physical damage

3.1. Damage assessment

The damage assessment considers physical flood damage to both the building envelope and structural framing of the prototype industrial building including metal wall siding, fenestrations (windows, personnel entry doors, overhead roller doors), steel portal frames and end wall frames. These were deemed the major subassemblies susceptible to flood

Fig. 1. Plan view of the prototype industrial building [35].

Table 1
Design specifications for critical building components.

Building component	Design specification
Wall siding panel	Stramit Monoclad® ribbed metal panels with 0.48 mm BMT, double-span, valley fixed to girts without cyclone caps. 0.76 m width × 2.75 m height
Wall girt	Stramit Z-section Z150-24 for long wall.Stramit Z-section Z300-24 for end wall.1.3 m spacingOne row bridging.
Steel frame member	Grade 300 460UB82 for rafters including haunch (total depth = 0.89 m)Grade 300 610UB125 for portal columnsGrade 300 410UB59 for end wall columns
Column base connection	4 ×M30 4.6/S hold down bolts to concrete footings for portal columns4 ×M24 4.6/S hold down bolts to concrete footings for end wall columns
Roof strut	Square tube SHS Grade 350 – 100 × 100 × 5.0
Roof and wall bracing	Equal angle tension ties 100 × 100 × 6 for roof bracingEqual angle tension ties 75 × 75 × 6 for wall bracing
Fenestration(doors, windows)	Fenestration is not specifically designed but their capacities are estimated later for the damage assessment (seeSection 3.3.2).

actions based upon observations in post-flood damage surveys (e.g., [12,23]) and engineering judgement. The water contact/contamination damage to building exterior, interior and contents is not explicitly considered in this section as the focus here is on physical building damage caused by flood forces. However, building interior losses are discussed further in Section 4. The flood actions considered to cause building damage are hydrostatic and hydrodynamic forces. The effects of wave (typically associated with coastal floods for buildings very close to shoreline), debris, erosion and scour of foundation are left for future studies. The inundation depth is assumed not to exceed the eave height of the building, and hence roof damage is not considered herein.

In this study, the physical damage of a non-structural subassembly (wall siding or fenestration), D_N (H, V), in the building envelope is measured by the probability of damage ratio, DR, as a function of flood intensities given by

$$D_N(H,V) = \Pr[DR|H,V] \tag{1}$$

where the flood intensity measures include inundation depth H and flow velocity V. For these subassemblies, the damage ratio is defined as the ratio between the number of damaged elements, e.g., wall panels, to the total number of those elements, e.g., total number of wall panels.

Steel portal framed industrial buildings generally lack redundancies [21,26]. Any structural component failure may trigger load redistribution and progressive damage of the structural system, which results in a partial or complete collapse of the building. Even if no collapse occurs, any building with structural damage is very likely unsafe to occupy and subjected to a loss of functionality. To this end, the physical damage of a structural subassembly (portal frames or end wall frames), D_S (H, V), is measured by the probability that at least one portal frame or end wall frame fails conditional on flood intensities:

$$D_S(H,V) = \Pr[\text{Any frame failure}|H,V] \tag{2}$$

The failure of either a single structural or non-structural component (e.g., a metal wall siding panel or a steel portal frame member) in the corresponding building subassembly is governed by the following limit state function:

$$g = C_R - L_D \tag{3}$$

where C_R is the component capacity, and L_D is the load effect (demand) on the component from flood and dead loads. A component fails if $g < 0$. The probability models of C_R and L_D are described in Section 3.3. The analyses for obtaining the structural demands/responses are 2D static for both the building envelope and structural framing. For structural framing, the supports and interactions from other structural elements (e.g., purlins, fly braces, cross-bracing systems) in the out-of-plane direction are also modelled in the 2D structural analysis. Details for assessing failures using Eq. (3) can be found in Section 3.3.

3.2. Flood loads

When water flow approaches in a direction perpendicular to the longitudinal axis of the prototype industrial building, the hydrostatic and hydrodynamic pressures acting on the long walls as well as the vertical hydrostatic pressures (buoyancy) acting on the concrete slab and footings are assumed to act as depicted in Fig. 3. The lateral hydrostatic pressures act inward and normal to all wall surfaces (front, back and side walls). If it is dry inside the building, the lateral hydrostatic pressure $P_S(X)$ at a height of X ($0 \le X \le H$) is computed as

$$P_S(X) = \rho_w g(H - X) \tag{4}$$

where ρ_w is the density of floodwater, g is the gravitational acceleration and H is the inundation depth outside the building. If floodwater enters the building, the hydrostatic pressure is reduced accordingly depending on the water depths on both sides of the wall. Given the water depth inside the building h ($h \le H$), see Fig. 3, the lateral hydrostatic pressure $P_S(X)$ at a height of X ($0 \le X \le H$) is computed as

$$P_S(X) = \begin{cases} \rho_w g(H - X) & h < X \le H \\ \rho_w g(H - h) & X \le h \end{cases} \tag{5}$$

When the flow direction is perpendicular to a wall, the hydrodynamic pressure P_D on the wall can be estimated as [14].

$$P_D = \frac{1}{2} C_d \rho_w V^2 \tag{6}$$

where C_d is a drag coefficient that depends on the ratio of building width (B) to inundation depth (H) [14], and V is the flow velocity. The C_d values (bounded by 1.25 and 2.0) for various B/H ratios are given by Table 6.10–1 in ASCE 7–16 (2017) with intermediate values obtained by linear interpolation. Suction pressures from hydrodynamic actions on side and back walls are conservatively neglected because they are considerably smaller than and acting in the opposite direction to the positive pressures by hydrostatic actions (inferred from [16]). As such, hydrodynamic forces are only considered on the front wall of the building.

The lateral flood force on a wall can be obtained by integrating the hydrostatic and/or hydrodynamic pressures given by Eqs. (4–6) over the wall surface area submerged in the floodwater. If the flow direction is not perpendicular to the wall, the hydrodynamic force is projected to the orthogonal direction multiplying a factor of $\sin^2\alpha$, where α is the horizontal angle between the flow direction and the wall surface. The buoyancy force (hydrostatic action in vertical direction) is not considered as an issue here. This is consistent with post-disaster observations that buildings with concrete floor slab and footings generally have satisfactory performance to resist floatation and movement during flood events [1,16,25].

3.3. Failure mechanism, demand and capacity modelling

3.3.1. Wall siding

The prototype industrial building has double-span metal wall panels (0.76 m width × 2.75 m height) supported by Z-section metal girts at 1.3 m spacing, and there are two rows of wall siding panels over the building height. Wall siding panels supported by girts are subjected to inward pressures from hydrostatic and/or hydrodynamic flood actions. Wall siding panel damage occurs if the inward pressures cause failures of the supporting girts or exceedance of the panel's yield and tensile strengths. According to building damage surveys (e.g., [23]) and engineering judgement, the former failure mode is more likely and typically occurs before the later. Hence, this study considers the damage of a metal wall panel caused by the failure of any girt supporting the panel

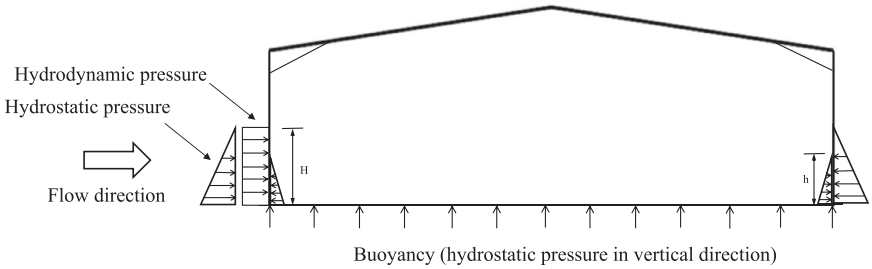

Fig. 3. Diagram of flood actions on the prototype industrial building.

under hydrostatic and hydrodynamic loads. The probability distributions and statistical parameters for the inward capacity of girts (kN/m) are shown in Table 2. The flood demand (kN/m) on a girt is approximately obtained by multiplying the area-averaging (averaged over the girt tributary area) pressure (kPa) from hydrostatic and hydrodynamic actions (only hydrostatic actions apply to side and back walls) by the girt tributary width (m) over the column height.

3.3.2. *Fenestration*

The windows, entry doors and overhead roller doors are all designed to resist uniform wind pressures. Windows and overhead roller doors need to satisfy the minimum test pressure for wind loads specified in AS2047 (Standards Australia 2014) and AS/NZS4505 (Standards Australia 2012). The mean capacities are assumed to be 20 % higher than the minimum test pressures following the approach by FEMA (2014). A normal distribution and a coefficient of variation (COV) of 0.20 are further assumed to model the window and overhead roller door capacities, and the probability distribution and statistical parameters for entry door capacity are estimated from the tests by Leblais & Henderson [18], see Table 2.

It is assumed that the failure modes for fenestration subjected to flood actions are the same with those under wind pressures. The failure modes for windows are typically tensile failure of glass panels and damage to panel fixings, sash or frame connections [7]. The doors are most likely to suffer damage to locks and hinges [18]. For overhead roller doors, disengagement of door curtain from tracks and damage to track fixings are critical, which typically occur before tensile failure of door curtain [7]. The hydrostatic and hydrodynamic pressures (could be non-uniform and may only be distributed over part of the fenestration area when partially submerged) acting on fenestration, in most cases, cannot be directly used to compare with the capacities in Table 2 to determine failures because these capacities are based on testing pressures uniformly distributed over the entire fenestration area. To assess fenestration failures induced by flood pressures, a finite element analysis (FEA) approach is used in this study. Applying thin plate theory, a window glass panel or door panel/curtain is modelled by linear elastic shell elements in ANSYS (ANSYS Inc 2013). Fig. 4 shows the schematic diagram of window, entry door and overhead roller door as well as the boundary conditions assumed for window glass panels and steel door panels/curtains. Geometrical nonlinearity is considered in the FEA with both bending and membrane actions considered. The maximum stresses and/or the maximum reaction forces at boundary supports for a window glass panel or a door panel/curtain are obtained from the FEA by respectively applying the flood pressure (hydrostatic and/or hydrodynamic pressures) and the uniform failure pressure (i.e., fenestration capacity in Table 2). The window failure is deemed to occur if either the maximum stress or the support reaction force induced by flood pressure exceeds that induced by the uniform failure pressure. The entry door and roller door failures are deemed to occur if the support reaction forces (at door locks, hinges or roller door tracks) induced by flood pressure exceed those induced by the uniform failure pressure. The proposed FEA approach is incorporated in the Monte Carlo simulation described in Section 3.4 to enable a probabilistic damage assessment for fenestration. Fig. 5 shows sample stress results from the FEA when the flow velocity is 2 m/s and the fenestration is just fully inundated (i.e., floodwater has the same height with the top edge of the fenestration).

3.3.3. *Portal frame*

For internal steel portal frames, the portal columns are subjected to critical internal forces induced by hydrostatic and hydrodynamic flood actions. The failure modes considered for a steel portal frame are bending failure of the column member and shear failure of the column base to concrete footing connection (i.e., hold down bolts). The column base connections are constructed and designed as nominally pinned according to Standards Australia (2020), and hence only shear failure of the hold down bolts are considered. Local buckling is not typically an issue for compact I-section columns (Standards Australia 2020) used for the prototype industrial building so is not considered further. The flexural buckling failure mode can also be ignored because the axial compression forces in frame members are relatively small. The spacings of girts on the portal columns are small enough to ensure out-of-plane lateral torsional buckling is also not an issue (Standards Australia 2020). The shear capacity of the I-section column member (see Table 1 for the member details) is much higher than the shear capacity of hold down bolts at the column base, and therefore the non-critical shear failure of column member is neglected.

The flood demands on a portal column are the maximum bending moment on the column member and the maximum shear force at the

Table 2
Probability models and statistical parameters for capacities of critical building components.

Building component		Mean	COV	Distribution type	Source
Wall girt		5.8 kN/m	0.15	Lognormal	Estimated based on manufacturer's design guide[44] and Stewart et al.[43].
Window		2.8kPa	0.20	Normal	Estimated based onAS 2047 andFEMA (2014)
Personnel door		3.4kPa	0.20	Normal	Estimated based onLeblais & Henderson[18]
Overhead roller door		3.1kPa	0.20	Normal	Estimated based on AS/NZS 4505 andFEMA (2014)
Roof strut		141 kN	0.20	Lognormal	Estimated based on Woolcock et al.[47] and Pham et al.[31]
End bay cross bracing	Roof bracing Wall bracing	386 kN 273 kN	0.10	Lognormal	Estimated based onASI[5] andPham[30]
Column member	Portal column End wall column	1236 kNm 432 kNm	0.10	Lognormal	Estimated based onASI[5] andPham et al.[31]
Column base connection	Portal column base End wall column base	669 kN 420 kN	0.10	Lognormal	Estimated based on AS4100 andPham & Hogan[32]

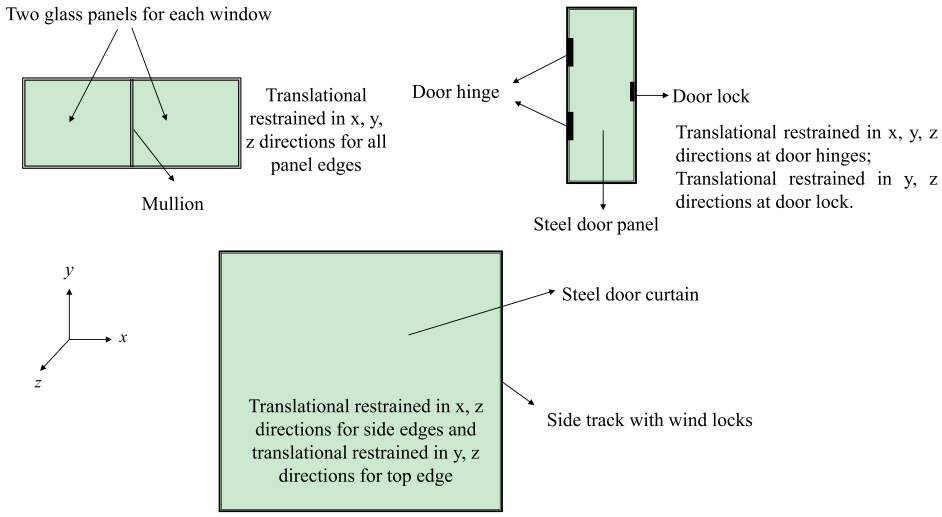

Fig. 4. Schematic diagram of fenestrations and boundary conditions in FEA.

column base. Nonlinear elastic structural analysis using finite element software ANSYS (ANSYS Inc 2013) is adopted to obtain the flood demands on portal columns given different combinations of inundation depth and flow velocity. If there is unbalanced floodwater inside the building, the induced hydrostatic loads will also be applied in the finite element analysis (FEA). In addition to internal forces induced by flood actions, the bending moment and shear force on a portal column due to loads arising from the self-weight of building components are also considered in the structural analysis. The FEA is adopted in a Monte Carlo simulation described in Section 3.4 for a probabilistic frame damage analysis. Note that, in the simulation, external flood loads on framing in the FEA will be modified if damage occurs to any building envelope supported by the frame.

A lognormal distribution is assumed for the moment capacity of the portal column member. The nominal moment capacity, mean-to-nominal ratio and coefficient of variation (COV) are obtained based on the design capacity tables given by ASI [5] and the statistics in Pham et al. [31]. Table 2 shows the probabilistic capacity model for the portal column member derived based on such statistical information. The design details of hold down bolts for the portal column base connection are given in Table 1 for the prototype industrial building. The nominal shear capacity of four M30 4.6/S bolts is calculated based on AS4100 (Standards Australia 2020). A lognormal distribution is assumed for the shear capacity of the portal column base connection with the mean-to-nominal ratio and COV obtained from Pham & Hogan [32]. Table 2 shows the probabilistic capacity model for the portal column base connection derived based on such statistical information.

3.3.4. End wall frame

End wall frame damage is considered to occur due to failures of the end wall columns and the bracing system (roof struts and end bay cross-bracing). End wall columns are subjected to bending failure of the column member and shear failure of the column base to concrete footing connection (i.e., hold down bolts) under flood loads. The probabilistic capacity models for the moment capacity for end wall columns and the shear capacity for column base connections are shown in Table 2. The roof struts are treated as beam-column members subjected to axial compression and self-weight induced bending. The effective length of a roof strut is taken as 5.72 m (i.e., frame spacing). The nominal roof strut capacities are expressed as axial compression capacity with the consideration of capacity reduction due to bending induced by self-weight, which can be obtained from Woolcock et al. [47] according to the designed member size and effective length of the roof strut. Considering a mean-to-nominal ratio of 1.20 and a COV of 0.20 [31], the probability model (lognormal distribution assumed) and statistical parameters for roof strut capacity are shown in Table 2. The end bay cross-bracing (roof and wall braces) are subjected to tension force only with the nominal tension capacity, mean-to-nominal ratio and coefficient of variation (COV) obtained from the design capacity tables given by ASI [5] and the statistics in Pham [30]. Table 2 shows the probabilistic capacity models (lognormal distribution assumed) for end bay roof and wall braces.

The flood demands on an end wall column are the shear force at the column base and the maximum moment on the column member. The end wall column is modelled as a simply supported beam (length L) subjected to hydrostatic and hydrodynamic loads as shown in Fig. 6. The hydrostatic load (kN/m) either inside or outside the building is calculated by multiplying the hydrostatic pressure computed from Eq. (4) by the tributary width of the column (i.e., 9.15 m). The hydrodynamic load is calculated by multiplying the hydrodynamic pressure computed from Eq. (6) by the tributary width of the column (the factor $\sin^2\alpha$ will also apply given oblique flow direction relative to the wall). The reactions at the top (R_{top}) and bottom (R_{base}) of the column as well as the maximum moment on the column are then derived analytically for different flood load scenarios depending on inundation depth, flow velocity, flow direction and water level difference inside and outside the building.

The shear force at the column base has an equal magnitude to the reaction at the bottom (R_{base}). Flood-induced inward force on the connection of roof strut to end wall column has an equal magnitude with the reaction at the top (R_{top}). Given the inward forces acting on these connections, the axial forces on roof struts and end bay cross-bracing can then be analytically obtained using the method of joints by considering roof struts as compression only members, and roof and wall braces as tension only members.

3.4. Load cases and Monte Carlo simulation

The hydrostatic load is a function of the difference between water depths inside and outside the building. The water depth difference during a flood event mainly depends on the outside flood rising rate and the water infiltration through small openings of the building envelope and breaches of the building envelope if wall siding and/or fenestration damage occurs. This study initially considers two bounding load cases for hydrostatic and hydrodynamic actions with respect to the water depth difference and the effect of building envelope damage.

Bounding case I: The building has equalized water depths inside and outside, and hence only hydrodynamic loads apply. This case may occur during slow-rise floods (generally riverine flooding) or when the

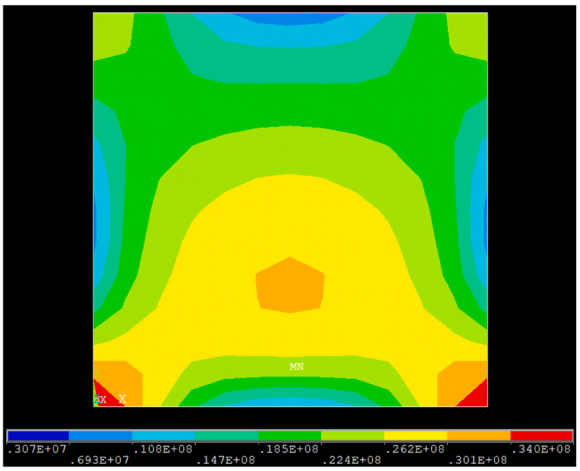

(a) One glass panel of a window

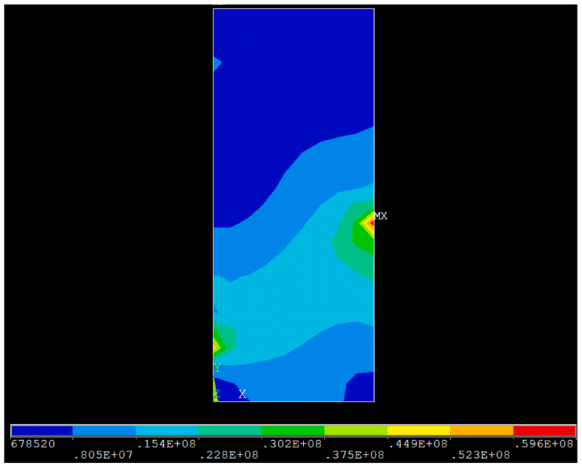

(b) Door

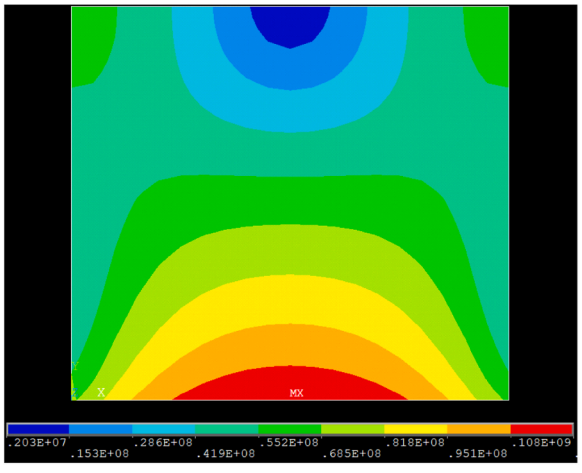

(c) Roller door

Fig. 5. Sample stress results from FEA.

building is wet-proofed.

Bounding case II: The building has negligible water inside, and therefore the full hydrostatic load as well as hydrodynamic load are applied to the outside of the building. However, if there are breaches of the building envelope, it is assumed that floodwater will quickly rise inside so that the hydrostatic loads are then cancelled, and only hydrodynamic loads apply to the structural components (as in bounding case I). This case may occur during rapid-onset floods (e.g., flash flooding, high-intensity coastal flooding) or when the building is dry-proofed.

The reality of a real flood event may lie somewhere in between these two bounding cases, i.e., floodwater enters the building, and differences between water depths inside and outside exist. Such water depth difference is hard to quantify with any real certainty, given that the flood rising rate outside the building (influenced by many factors such as flood type, terrain, surrounding built environment and local drainage system) and the water infiltration rate into a metal-clad industrial building are relatively unknown and likely to be variable for different structures. Hence, in addition to the bounding cases, a sensitivity analysis considering a range of internal water depths is also conducted to examine the effect of water depth difference on flood induced physical damage.

The damage assessment is carried out probabilistically using Monte Carlo simulation (MCS) considering the inundation depth ranging from 0.2 m to 5 m (0.2 m increment) and the flow velocity ranging from 0 m/s to 6 m/s (0.5 m/s increment). The inundation depth and flow velocity are treated as deterministic values. Three flow directions, $\varphi = 0°$, 45° and 90° (Fig. 2), relative to the longitudinal building axis are considered. As the prototype industrial building is symmetrical, the physical damage obtained under the three flow directions can be used for mirrored flood approaching angles. For each combination of inundation depth, flow velocity, flow direction and flood load case, 5000 simulation runs are conducted (a total of 9750,000 simulation runs) to obtain 5000 random samples of physical damage ratios for different building subassemblies, which are then integrated and converted to the overall building loss ratio through a vulnerability assessment described in Section 4. Fig. 7 shows a flowchart for the MCS analysis.

4. Vulnerability assessment

An assembly-based approach (e.g., [33]; FEMA 2014; [34]) is adopted here for the vulnerability assessment. This approach integrates monetary losses resulting from the physical damage of different building subassemblies. Building interior losses due to floodwater inundation are also considered by using existing stage-depth damage curves (e.g. USACE 2006). The expected building loss ratio (ratio of the damage repair or replacement cost to the building value) as a function of flood intensities (inundation depth H and flow velocity V) is used here as a measure of the building vulnerability, which is given by

$$VN(H,V) = \sum_{i=1}^{N} [CR_i \times E(LS_i|H,V)] \tag{7}$$

where $VN(H, V)$ is the building vulnerability, N is the number of building subassemblies considered in the vulnerability assessment, CR_i is the cost ratio of the i^{th} subassembly defined as the ratio of the repair or replacement cost for the entire i^{th} subassembly to the building value (i.e., the cost to construct a new building), $E(LS_i \mid H, V)$ is the expected loss ratio (LS_i) of the i^{th} subassembly (ratio of the damage repair or replacement cost for the i^{th} subassembly to the cost for repairing or replacing the entire subassembly) conditional on flood intensities. Table 3 shows the cost ratios for building subassemblies estimated from Australian construction cost guide [36]. The summation of these cost ratios is greater than 100 % of the building value because of the extra costs associated with repair, removal and replacement works following a flood event. These extra costs are assumed to be 25 % of the original value in this study, though the actual costs after a flood event may vary. If the building replacement value is used for the normalization of cost ratios, then it adds up to 100 %.

For subassemblies in the building envelope such as wall siding and fenestration, the expected loss ratio of the i^{th} subassembly, $E(LS_i \mid H, V)$, equals to the mean physical damage ratio of this subassembly, $E(DR_i \mid H, V)$, that can be obtained from the damage assessment described in

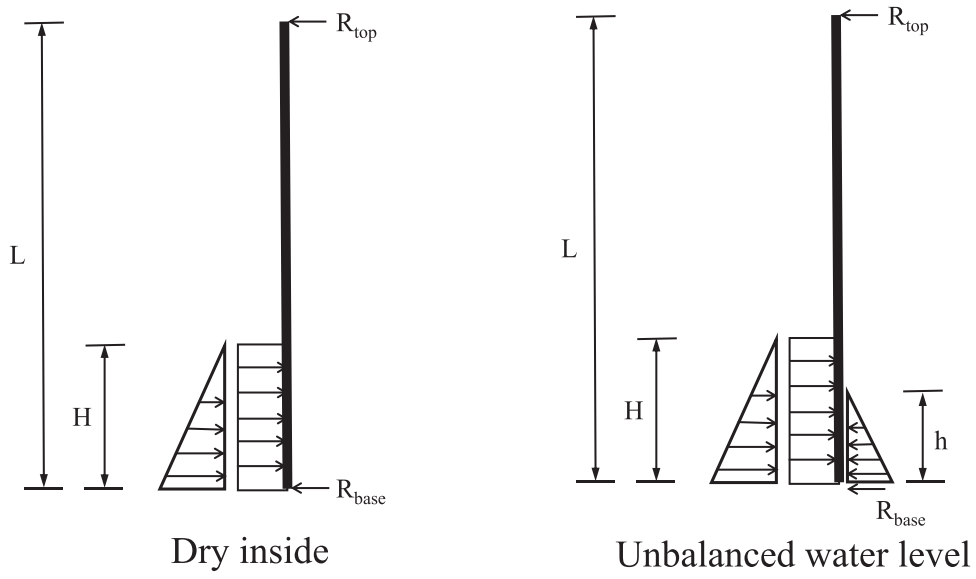

Fig. 6. Flood loads on an end wall column.

Section 3. For building interior, the loss is due to floodwater inundation inside the building, which is a function of inundation depth. It is assumed that the water depth inside the building will eventually equal to the outside inundation depth (regardless of the load cases described in Section 3.4) for a flood event (usually longer than 24 h). In this study, the expected loss ratio of the building interior as a function of inundation depth is estimated from the loss tables in USACE (2006) and expressed as a stage-depth curve shown in Fig. 16 together with the vulnerability analysis results. No foundation losses are considered in this study.

For structural framing, only the occurrence probability of structural failure is assessed in the damage assessment. The exact consequences after the initiation of structural failure are not explicitly modelled so it is not clear whether the structural failure remains local or triggers a progressive collapse of other structural frames. Based on expert judgement, the loss ratio of structural framing given the occurrence of structural failure is then assumed to follow a triangular probability distribution. According to the damage assessment results in Section 5.1.2, end wall frame failure and portal frame failure are unlikely to occur simultaneously for a given flow direction. If an end wall frame fails, the triangular probability distribution is assumed to have a mode of 0.25, a lower bound of 0.10 and an upper bound of 0.50. Thus, the expected loss ratio of structural framing given an end wall frame failure is 0.28 (i.e., the mean of the triangular distribution) that contributes $0.28 \times 37\ \% = 10.4\ \%$ to the expected building loss ratio. If failure occurs to steel portal frames, the triangular probability distribution is assumed to have a mode of 0.60, a lower bound of 0.20 and an upper bound of 1.0. Hence the expected loss ratio of structural framing given portal frame failure is 0.60 (i.e., the mean of the triangular distribution) that contributes $0.60 \times 37\ \% = 22.2\ \%$ to the expected building loss ratio.

5. Results

The physical damage and vulnerability analyses generate results that are essentially 3D surfaces in terms of flood inundation depth and flow velocity. These results could be presented as surfaces, and they could be integrated over all the flow directions or could be presented separately for each flood direction. All the results in this section are presented as 2D curves that are snapshots from the 3D surface where one of the flood parameters has been fixed. In this way, we believe the physical damage and vulnerability results can be better interpreted by revealing the influences of different flood parameters and load cases.

5.1. Physical damage of building subassemblies

5.1.1. Building envelope

The damage assessment was conducted for the building envelope (wall siding and fenestrations) considering the two bounding cases. Figs. 8 and 9 show the mean damage ratios of wall siding and fenestrations respectively for various inundation depths and flow velocities considering flow approaching in the direction of $\varphi = 90^{\circ}$ (see Fig. 2) relative to the longitudinal building axis (i.e., transverse direction - flow perpendicular to the long wall). The figures suggest that, as expected, the mean damage ratios of wall siding and fenestrations generally increase with inundation depth and flow velocity. The damage ratios corresponding to Bounding case II are higher than those corresponding to Bounding case I because load case II has combined hydrostatic and hydrodynamic actions, while for load case I, only hydrodynamic loads apply to the building envelope. The wall siding and fenestrations reach full damage when the inundation depth is around 3.6 m for Bounding case II. For Bounding case I, the mean damage to wall siding and fenestration initiates at 2.5 m/s and 2 m/s, respectively. For Bounding case II, the damage curves for wall siding and fenestration have six stages as the inundation depth increases (indicated by the numbers in Figs. 8 and 9). In Stage 1, flood damage mainly occurs to the lower row of wall siding panels (two rows of wall siding panels along the building height as described in Section 3.3.1), the entry doors and roller doors (see Fig. 1) facing the floodwater flow that are subjected to combined hydrostatic and hydrodynamic actions. The slope of damage curve (i.e., increasing rate of damage with inundation depth) considerably increases with flow velocity. In Stage 2, flood damage starts to occur to the lower row of wall siding panels, the entry doors and roller doors not facing the floodwater flow. As only hydrostatic loads apply, the slopes of damage curves are comparable for different flow velocities. In Stage 3, the maximum possible damage to the lower row of wall siding panels, the entry doors and roller doors occur. In Stage 4, flood damage again increases as the inundation depth increases when floodwater reaches the upper row of wall siding panels and the windows (see Fig. 1). The damage in this stage mainly occurs to the building envelope facing the flow with combined hydrostatic and hydrodynamic actions. In Stage 5, the damage starts to occur to the upper row of wall siding panels and the windows not facing the flow with hydrostatic loads only, and it reaches the maximum possible damage ratio in Stage 6. In general, the damage curves for the building envelope are more sensitive to flow velocity when the inundation depth for relevant non-structural components is

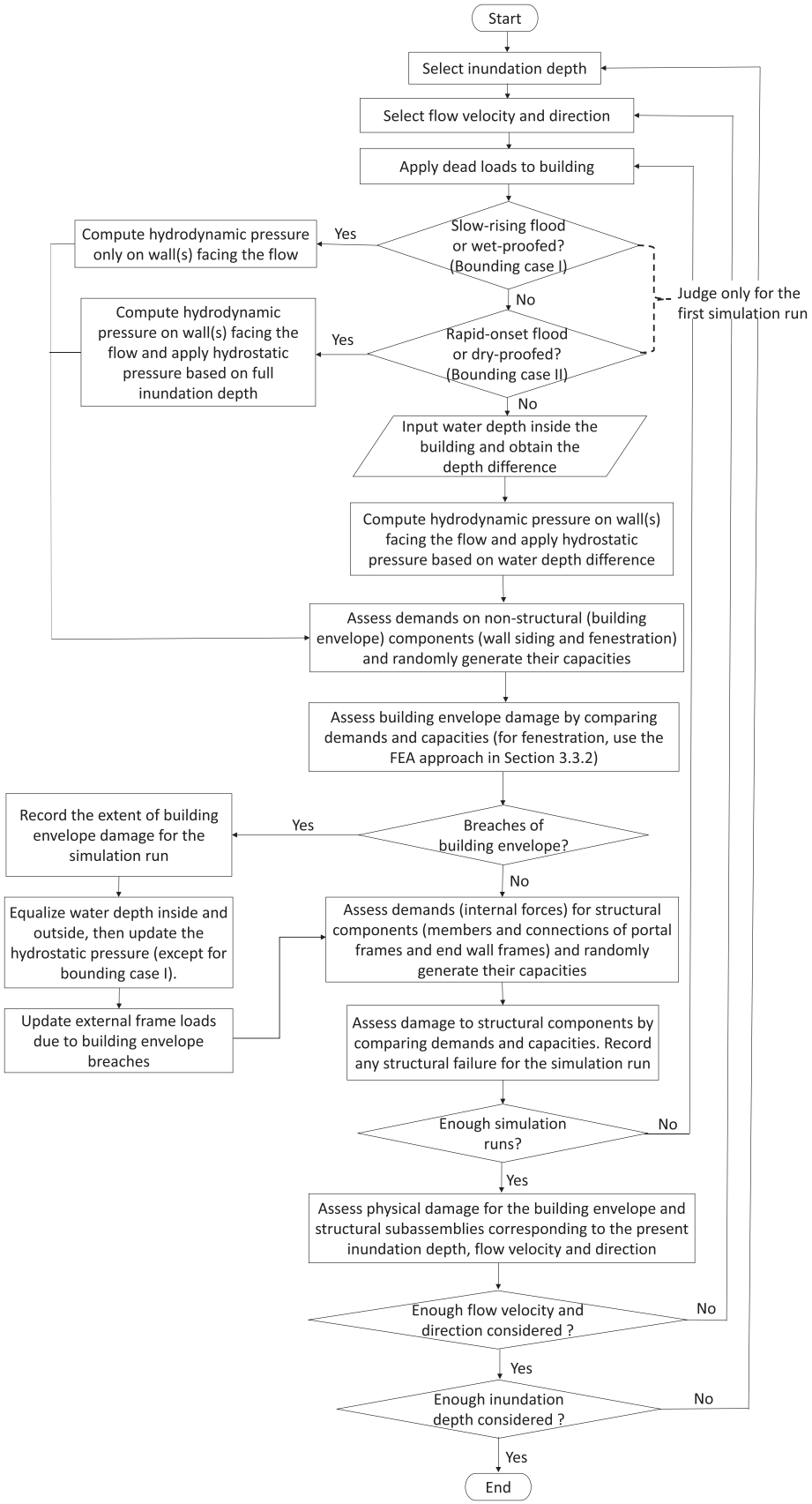

Fig. 7. MCS flowchart for flood damage assessment.

Table 3
Subassembly cost ratios for the prototype industrial building.

Subassembly		Description	Cost ratio	Total
Foundation		Concrete footings and slab	28 %	
Building envelope	Roof cladding	Metal roof panels and purlins	9 %	
	Wall siding	Metal wall panels and girts	7 %	
	Fenestration	Windows, entry doors and overhead roller doors	4 %	
Structural framing		Steel portal frames, end wall frames and bracing systems	37 %	125 %
Building interior	Internal construction and finishes	Wall lining and flooring with finishes	6 %	
	Mechanical	HAVC, plumbing and fire safety system	25 %	
	Electrical	Lighting and power systems	9 %	

relatively low, because in this case, hydrodynamic actions have more contributions to the failures of these non-structural components. The transition to different stages occurs at lower inundation depths as flow velocity increases. For Bounding case I with equalized water depths inside and outside, only Stage 1, 3, 4 and 6 apply to the damage curves (see Figs. 8 and 9), and damage is only incurred by hydrodynamic loads on the long wall under a transverse flow direction with damage ratio therefore capped at around 36 % and 39 % for wall siding and fenestrations, respectively.

Figs. 10 and 11 examine the effect of flow direction on wall siding and fenestration damage. For Bounding case II, the differences between damage curves for the three flow directions are not significant because hydrostatic force is the governing flood action. For Bounding case I, as only hydrodynamic loads apply, the damage curves are sensitive to flow directions. A flow direction of 90° (i.e., transverse direction, flow perpendicular to the long wall) leads to higher damage ratios of wall siding and fenestration than the 0° direction (i.e., longitudinal direction, flow perpendicular to the end wall) because more wall siding panels, windows and doors are impacted by hydrodynamic actions under the 90° direction. Among the three flow directions, the 45° direction has the largest building envelope area impacted by hydrodynamic actions because wall siding and fenestration on both the long wall and end wall are subjected to hydrodynamic loads. However, the hydrodynamic loads projected to the long wall and end wall under the 45° direction are lower than those under the two orthogonal flow directions. Thus, the building envelope damage for the 45° direction is generally lower than those corresponding to the two orthogonal flow directions for relatively low and moderate flow velocities (i.e., 1 m/s and 3 m/s) where forces do not exceed failure thresholds but higher for a relatively high flow velocity (i.e., 5 m/s) where forces on components are high (and exceed failure thresholds) and there are more of them to damage.

5.1.2. *Structural framing*

This section presents the damage probabilities for structural framing (portal frames and end wall frames) considering the two bounding cases. It is assumed that the failure of the building envelope will always occur first during the process of flood rising because their resistances to flood loading are much lower than the structural framing in the current design

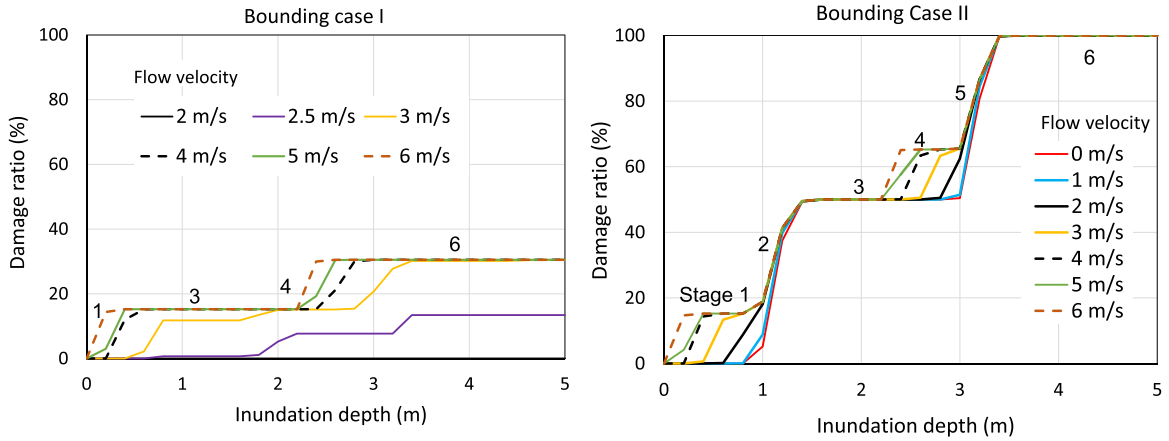

Fig. 8. Wall siding damage for various inundation depths and flow velocities considering two bounding load cases and a flow direction of 90° (transverse direction).

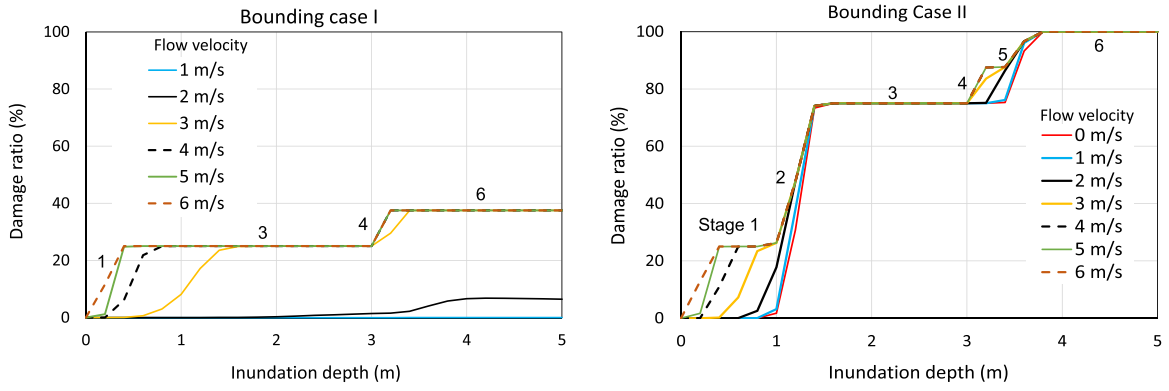

Fig. 9. Fenestration damage for various inundation depths and flow velocities considering two bounding load cases and a flow direction of 90° (transverse direction).

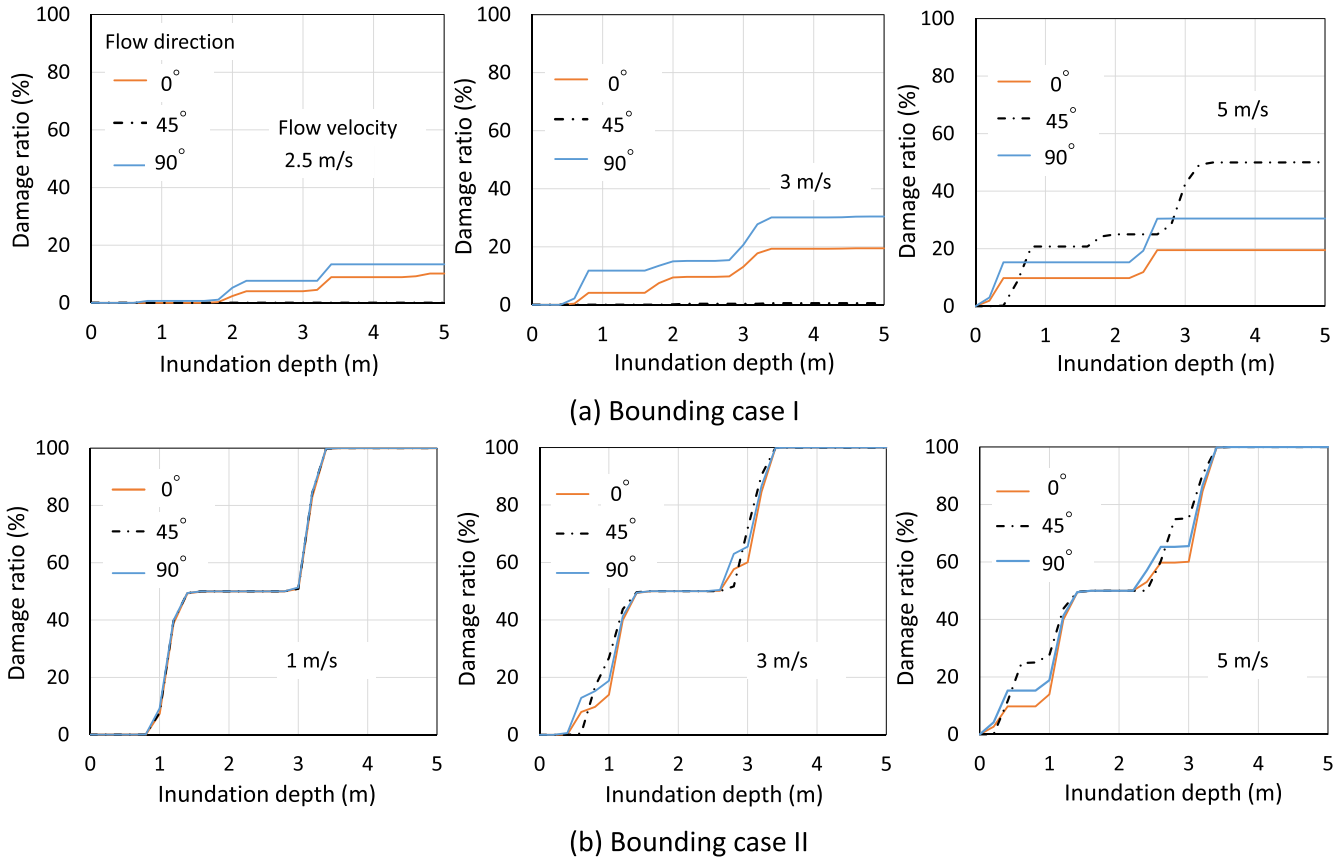

Fig. 10. Effects of flow direction on wall siding damage for the two bounding load cases.

and construction practice. After breaches of the building envelope, floodwaters are assumed to have entered the building, and water depths inside and outside the building are equalised and therefore hydrostatic loads on framing are cancelled. Hence, the portal frame and end wall frame are mainly subjected to hydrodynamic loads. The flood loads on framing are also reduced at the breaches of building envelope due to reduced tributary area of framing. This means that structural failures are relatively rare and for the steel portal frame were only found to occur for the highest flow velocity of 6 m/s and the flow direction of 90° (i.e., flow perpendicular to the long wall) with inundation depths over 4 m (see Fig. 12(a)). As such, the portal frame damage curves are identical for the two bounding cases in Fig. 12(a). It was also found the shear failure of column base connections is a more critical failure mode.

Fig. 12(b) shows end wall frame damage probabilities under the critical flow direction of 0° (i.e., flow perpendicular to the end wall) considering the two bounding load cases. Like the portal frames, end wall frame failures are only induced by hydrodynamic actions after building envelope damage occurs and there are no differences between damage curves for the two bounding cases because of this (shown in one figure). The lowest flow velocity for end wall failure to occur is around 2 m/s with the inundation depth over 4 m. Under the highest flow velocity of 6 m/s, end wall failure begins to occur at an inundation depth around 1.2 m. Fig. 13 examines the effect of flow direction on end wall frame damage. Under the flow direction of 90°, there is no failure as no hydrodynamic loads take effects on the end wall frame. Damage probabilities for the flow direction of 45° are lower than those corresponding to the 0° direction because the hydrodynamic loads on end wall frame are lower. However, such difference decreases as flow velocity increases.

5.1.3. *Influence of water depth difference*

This section examines the effects of differing water depths inside and outside the building on assembly flood damage. Water depths inside the building of 100 % (Bounding case I), 75 %, 50 %, 25 % and 0 % (Bounding case II) of the outside inundation depth are examined. Given failures of structural framing may only occur following envelope breaches (Section 5.1.2), at which time equilibration of internal and external water levels could largely be ensured, the effects of water depth difference are only examined for building envelope damage. Figs. 14 and 15 show the mean damage ratios of wall siding and fenestration considering different scenarios of inside water depth for a flow direction of 90°. These figures show that the larger the water depth difference (or the lower the inside water depth), the higher the damage ratios of the building envelope. The differences between the damage curves corresponding to various inside water depths decrease with flow velocity, which is expected as hydrodynamic actions contribute more to the damage as flow velocity increases. Large differences between the damage curves corresponding to various inside water depths (except for Bounding case I) tend to occur when the inundation depths are around 1 to 2.5 m as the effects of hydrostatic actions are high within this range of inundation. It is shown that the difference over this inundation range is most substantial when the inside water depth exceeds 50 % of the outside inundation depth, with the damage being largely comparable when internal water depth is below 50 %. Little difference is seen between all curves for external depths of > 2.5 m when some level of asymmetry in the internal and external depths is evident. This is because, exceeding this inundation depth, even the smallest water depth difference (i.e., inside water depth is 75 % of the outside inundation depth) could impose considerable hydrostatic forces on the building to cause significant wall siding and fenestration damage. It also indicates that wall siding damage is more sensitive to the water depth difference than the fenestration damage.

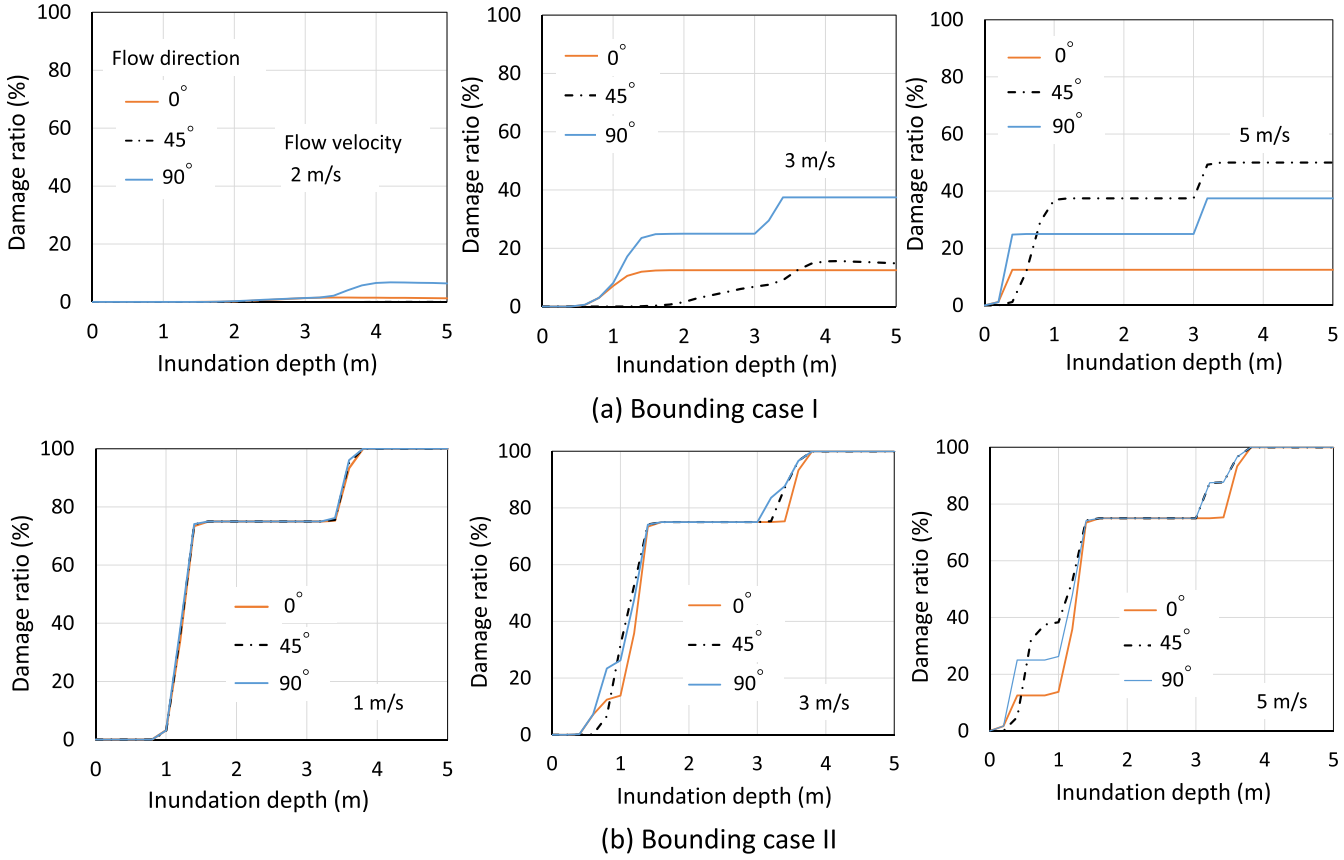

Fig. 11. Effects of flow direction on fenestration damage for the two bounding load cases.

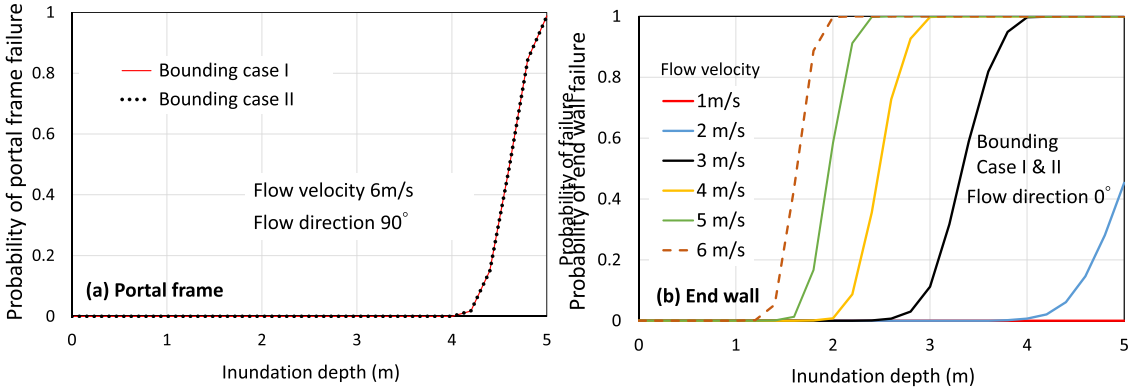

Fig. 12. Structural framing damage probabilities considering two bounding load cases.

5.2. *Building vulnerability*

Fig. 16 shows the building vulnerability considering the two bounding load cases and two orthogonal flow directions (0° and 90°). The building interior loss (estimated based on USACE 2006) as a function of inundation depth (not dependant on flow velocity) is also shown in the figures and can be viewed as the lower bound for loss ratios for a given inundation depth. The gap between a vulnerability curve and the interior loss curve represents the losses of the building envelope and structural framing.

For the longitudinal flow direction perpendicular to the end wall (i.e., 0°), the higher the flow velocity, the higher the contribution of building envelope damage and end wall frame failure to the building vulnerability. For the bounding load case I, relatively low flow velocities only lead to building interior losses from floodwater inundation because the hydrodynamic loads are not significant enough to cause damage to other building subassemblies. For the bounding load case II, due to the presence of hydrostatic loads, building losses from damage to subassemblies other than building interior also exist for relatively low flow velocities. The sudden increases in building loss ratios seen in many of the curves appear due to the occurrence of end wall frame failure at relatively high flow velocities (i.e., 2–6 m/s).

For the transverse flow direction perpendicular to the long wall (i.e., 90°), the building vulnerability is less sensitive to flow velocities except for the flow velocity of 6 m/s. This is because portal frame failure only occurs for extreme flood conditions (i.e., the highest flow velocity of 6 m/s considered in the damage assessment with inundation depths over 4 m, see Fig. 12(a)), which cause this sudden increase of the building

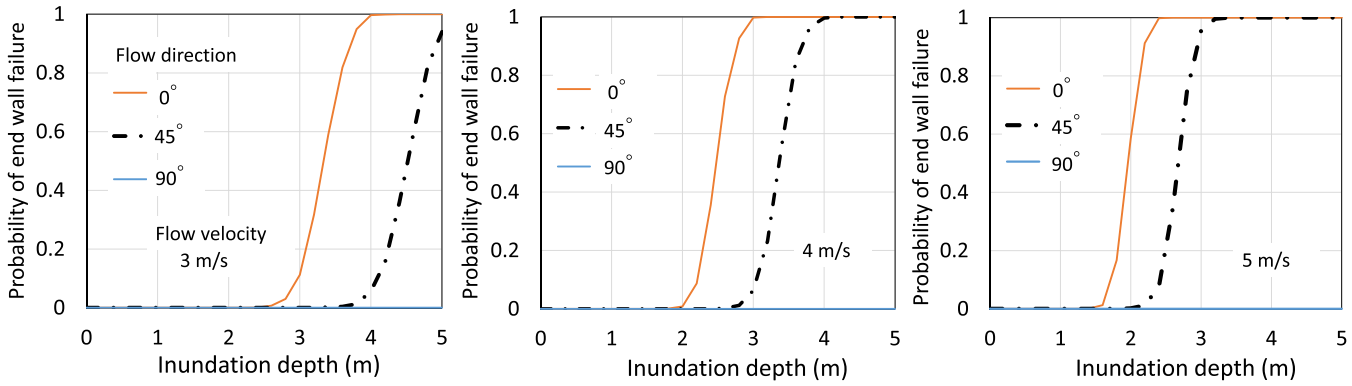

Fig. 13. Effects of flow direction on end wall frame damage.

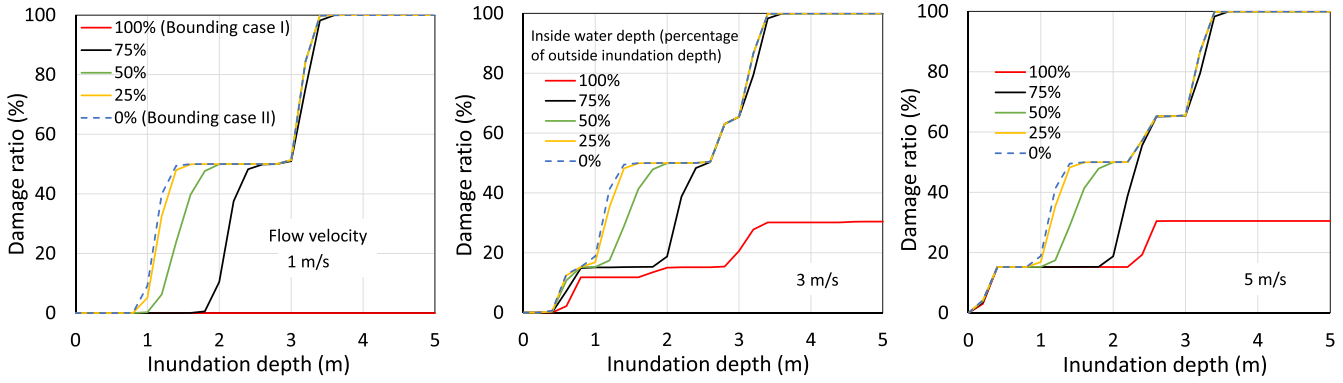

Fig. 14. Wall siding damage considering different scenarios of inside water depth.

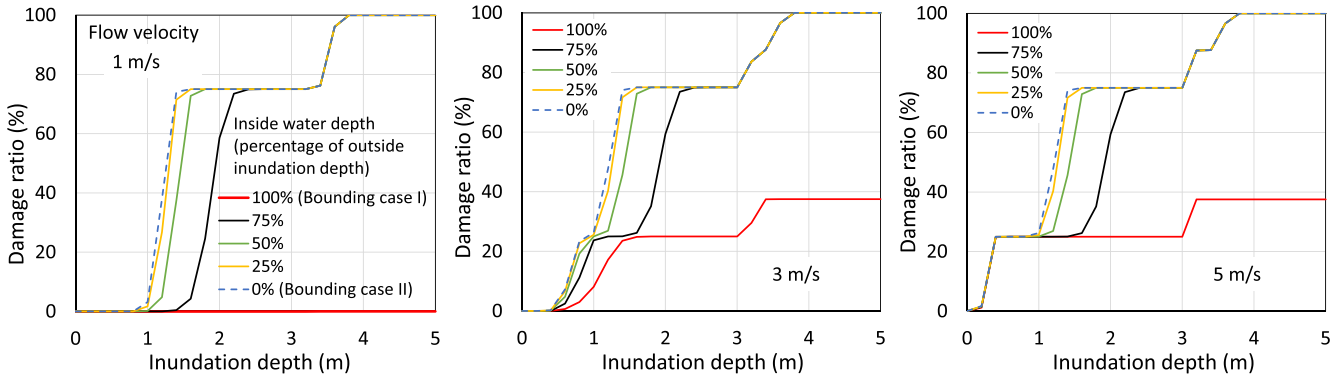

Fig. 15. Fenestration damage considering different scenarios of inside water depth.

vulnerability curve corresponding to a flow velocity of 6 m/s. The combined repair/replacement cost of wall siding and fenestration is only 11 % of the building value (see Table 3) which is less significant compared to other building subassemblies (e.g., building interior, structural framing). This fact explains why when no portal frame failure occurs, the differences between building vulnerabilities corresponding to different flow velocities (the gap between a vulnerability curve and the interior loss curve) are not prominent.

6. Conclusions

This paper presents a physics-based vulnerability model for steel portal framed industrial buildings subjected to simplified hydrostatic and hydrodynamic flood actions. Physical damage induced by flood forces to the building envelope (wall siding and fenestrations) and the structural framing (steel portal frames and end wall frames) were considered. A Monte Carlo simulation was employed to conduct the damage assessment by incorporating various idealised flood load cases, probability models of demands and capacities as well as major failure mechanisms of different structural and non-structural components. The physical damage assessment was conducted for a prototype industrial building in Australia. The obtained damage curves express either the damage ratios of building envelope or the failure probability of structural framing as a function of inundation depth and flow velocity for different flow directions. An assembly-based vulnerability method was then used to convert physical damage ratios of individual building subassemblies into monetary building loss ratio for various inundation depths, flow velocities and flow directions. Building interior losses due

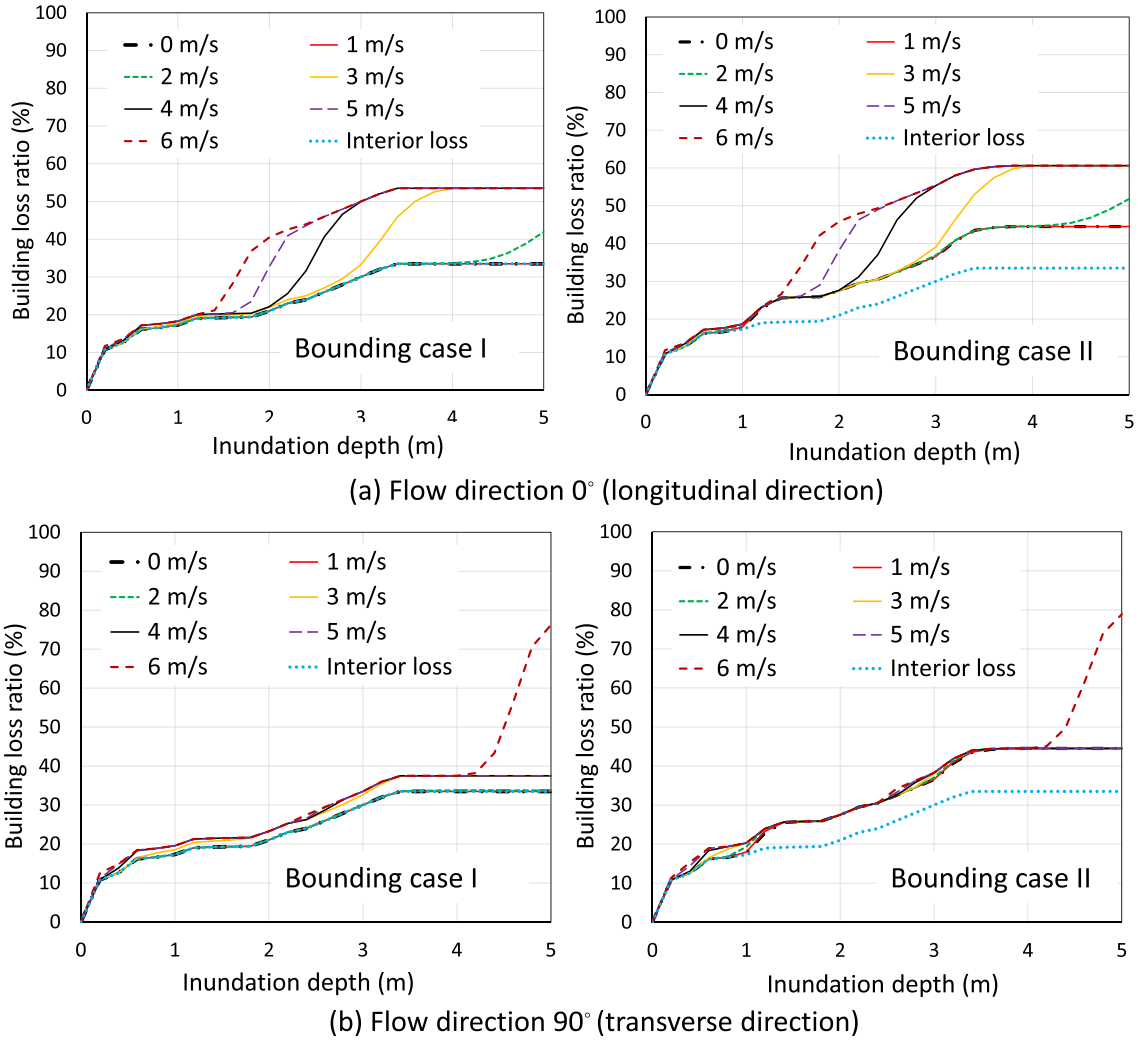

Fig. 16. Building vulnerabilities for various inundation depths and flow velocities considering two bounding load cases and two orthogonal flow directions.

to floodwater inundation were also considered by using existing stage-depth damage curves. The developed vulnerability model can be used to support flood risk management and resilience enhancement for industrial buildings.

The damage assessment for the prototype industrial building suggests that, as expected, the mean damage ratios of the building envelope generally increase with inundation depth and flow velocity. The wall siding and fenestration reach full damage when the inundation depth is around 3.6 m (approximately 65 % of the building height) if the building inside is dry. For equalized water depths inside and outside the building, the mean damage ratios for wall siding and fenestration only reach around 30–40 % even for relatively high flow velocities. The building envelope damage is more sensitive to flow directions when water depths are equal inside and outside the building as direction-dependent hydrodynamic actions govern. It was found from the analyses that flood damage to structural framing is caused only by hydrodynamic actions. This was the case because wall sidings or fenestrations always failed earlier during the rising of floodwater due to much lower resistances to flood loads. This leads to equalisation of water depths inside and outside the building and cancelled hydrostatic loads on structural framing. The flood loads on framing will also be reduced due to breaches in the building envelope resulting in reduced tributary areas of framing. End wall frames are the more vulnerable structural subassembly. When the flow approaches in a direction perpendicular to the end wall, the lowest flow velocity for end wall frame failure to occur is around 2 m/s with the inundation depth over 4 m. It was also found in the structural framing damage assessments that the shear failure of column base connections is a more critical failure mode. The assembly-based vulnerability assessment suggests that losses to structural framing and building interior have more significant contributions to the building vulnerability. Losses from end wall damage is more likely to occur for a longitudinal flow direction while portal frame damage only contributes to the building vulnerability under extreme flood loads and a transverse flow direction.

This study considered physical damage only induced by idealised flood load scenarios to major structural and non-structural components of industrial buildings. Future studies need to further develop physics-based models accounting for the effects of water contact/contamination, wave action (if the building is very close to shoreline), debris impact, and erosion and scour of foundation on building vulnerability. Better quantification of how water infiltrates into a building during flood events and how internal and external water depths vary with respect to each other and around a building is also needed to provide more reliable loading models for the physics-based models such as the one proposed here. Validation of the vulnerability model is only feasible when adequate flood damage data for this type of industrial buildings are collected from real flood events.

CRediT authorship contribution statement

Hao Qin: Writing – original draft, Visualization, Software, Methodology, Investigation, Formal analysis, Data curation, Conceptualization. **Matthew Mason:** Writing – review & editing, Supervision, Resources, Project administration, Methodology, Funding acquisition, Conceptualization. **Mark Stewart:** Writing – review & editing, Supervision, Methodology.

Declaration of Competing Interest

The authors declare that they have no known competing financial interests or personal relationships that could have appeared to influence the work reported in this paper.

Data Availability

Data will be made available on request.

Acknowledgement

Funding for this research was provided by the AXA Research Fund through the Joint Research Initiative. Discussions with Mr Mathis Joffrain and Prof. Hubert Chanson in defining and carrying out this research are also greatly acknowledged.

References

[1] Amirebrahimi S. Doctoral dissertation. The University of Melbourne, Australia. A Framew Micro Lev Assess 3D Vis Flood Damage A Build 2016.
[2] Amirebrahimi S, Rajabifard A, Mendis P, Ngo T. A framework for a microscale flood damage assessment and visualization for a building using BIM–GIS integration. Int J Digit Earth 2016;9(4):363–86.
[3] ANSYS Inc (2013). ANSYS Mechanical APDL Introductory Tutorials. Canonsburg, PA; USA.
[4] ASCE (2017). ASCE/SEI 7–16 Minimum design loads for buildings and other structures. American Society of Civil Engineer, Reston, VA, USA.
[5] ASI (1999). Design Capacity Tables for Structural Steel, Volume 1: Open Sections. 3rd edition, Australian Steel Institute, Sydney, Australia.
[6] Becker AB, Johnstone WM, Lence BJ. Wood frame building response to rapid-onset flooding. Nat Hazards Rev 2011;12(2):85–95.
[7] Boughton G. , Henderson D. , Ginger J. , Holmes J. , Walker G. , Leitch C. , et al. , et al. (2011). Tropical cyclone Yasi: structural damage to buildings. Technical Report No.57. Cyclone Testing Station, James Cook University, Australia.
[8] Custer R, Nishijima K. Flood vulnerability assessment of residential buildings by explicit damage process modelling. Nat Hazards 2015;78(1):461–96.
[9] De Risi R, Jalayer F, De Paola F, Iervolino I, Giugni M, Topa ME, et al. Flood risk assessment for informal settlements. Nat Hazards 2013;69(1):1003–32.
[10] Do TQ, van de Lindt JW, Cox DT. Hurricane surge-wave building fragility methodology for use in damage, loss, and resilience analysis. J Struct Eng 2020;146 (1):04019177.
[11] Dong Y, Frangopol DM. Probabilistic life-cycle cost-benefit analysis of portfolios of buildings under flood hazard. Eng Struct 2017;142:290–9.
[12] Eamon CD, Fitzpatrick P, Truax DD. Observations of structural damage caused by Hurricane Katrina on the Mississippi Gulf Coast. J Perform Constr Facil 2007;21(2): 117–27.
[13] FEMA (2009). Multi-Hazard Loss Estimation Methodology: Flood Model, Technical Manual. Federal Emergency Management Agency, Mitigation Division, Washington DC, USA.
[14] FEMA (2012). Engineering principles and practices for retrofitting flood-prone residential structures. FEMA P-259. Federal Emergency Management Agency, Washington DC, USA.
[15] FEMA (2014). Hazus Hurricane Model Technical Manual. Federal Emergency Management Agency, Mitigation Division, Washington DC, USA.
[16] HNFMSC (2006). Reducing Vulnerability of Buildings to Flood Damage: Guidance on Building in Flood Prone Areas. Hawkesbury-Nepean Floodplain Management Steering Committee, Parramatta, NSW, Australia.
[17] ICA (2022). Insurance catastrophe resilience report 2021–22. Insurance Council of Australia, Sydney, Australia.
[18] Leblais, A. & Henderson D. (2018). Simulated wind load strength testing of entrance doors. Bushfire and Natural Hazards CRC, Melbourne, Australia.
[19] Jalayer F, Carozza S, De Risi R, Manfredi G, Mbuya E. Performance-based flood safety-checking for non-engineered masonry structures. Eng Struct 2016;106: 109–23.
[20] Johnson F, White CJ, van Dijk A, Ekstrom M, Evans JP, Jakob D, et al. Natural hazards in Australia: floods. Clim Change 2016;139(1):21–35.
[21] Kareem A. Structural performance and wind speed-damage correlation in Hurricane Alicia. J Struct Eng 1985;111(12):2596–610.
[22] Kelman I. (2002). Physical flood vulnerability of residential properties in coastal, Eastern England. PhD Thesis, University of Cambridge, Cambridge, UK.
[23] Kijewski-Correa, T. , Prevatt, D. , Berman, J. , Mosalam, K. , Roueche, D. , Robertson, I. , & et al. (2020). StEER - Hurricane Michael, Dataset. PRJ2113, DesignSafe-CI, doi: 10.17603/ds2–5aej-e227.
[24] Kundzewicz ZW, Kanae S, Seneviratne SI, Handmer J, Nicholls N, Peduzzi P, et al. Flood risk and climate change: global and regional perspectives. Hydrol Sci J 2014; 59(1):1–28.
[25] Mason, M.S., Phillips, E., Okada, T.andO'Brien, J. (2012). Analysis of damage to buildings following the 2010–11 Eastern Australia floods. National Climate Change Adaptation Research Facility, Gold Coast, Australia.
[26] Mehta KC, Minor JE, Reinhold TA. Wind speed-damage correlation in Hurricane Frederic. J Struct Eng 1983;109(1):37–49.
[27] Nadal NC, Zapata RE, Pagan I, Lopez R, Agudelo J. Building damage due to riverine and coastal floods. J Water Resour Plan Manag 2010;136(3):327–36.
[28] NCC (2019). National construction code, Volume One. Australian Building Codes Board, Canberra, Australia.
[29] Paleo-Torres A, Gurley K, Pinelli JP, Baradaranshoraka M, Zhao M, Suppasri A, et al. Vulnerability of Florida residential structures to hurricane induced coastal flood. Eng Struct 2020;220:111004.
[30] Pham L. Safety index analyses of tension members. *Civil Engineering Transactions. Inst Eng Aust*, CE29 1987;(2):128–30.
[31] Pham L, Bridge RQ, Bradford MA. Calibration of the proposed limit states design rules for steel beams and columns. *Civil Engineering Transactions*. Inst Eng Aust 1986;CE28(3):268–74.
[32] Pham L, Hogan TJ. Calibration of the proposed limit states design rules for bolted connections. *Civil Engineering Transactions*. Inst Eng Aust 1986;CE28(4):292–7.
[33] Porter KA, Kiremidjian AS, LeGrue JS. Assembly-based vulnerability of buildings and its use in performance evaluation. Earthq Spectra 2001;17(2):291–312.
[34] Qin H, Stewart MG. Wind and rain losses for metal-roofed contemporary houses subjected to non-cyclonic windstorms. Struct Saf 2020;86:101979.
[35] Qin H, Mason M, Stewart MG. Fragility assessment for new and deteriorated portal framed industrial buildings subjected to tropical cyclone winds. Struct Saf 2023; 100:102287.
[36] Rawlinsons (2021). Rawlinsons Construction Cost Guide 2021. Rawlinsons Publishing, Perth, Australia.
[37] Salman AM, Li Y. Flood risk assessment, future trend modeling, and risk communication: a review of ongoing research. Nat Hazards Rev 2018;19(3): 04018011.
[38] Standards Australia (2002). Structural Design Actions, General principles. AS/NZS1170.0, Standards Australia, Sydney.
[39] Standards Australia (2012). Garage doors and other large access doors. AS/NZS4505, Standards Australia, Sydney.
[40] Standards Australia (2014). Windows and external glazed doors in buildings. AS2047, Standards Australia, Sydney.
[41] Standards Australia (2020). Steel structures. AS4100, Standards Australia, Sydney.
[42] Stewart MG, Rosowsky DV. Extreme Events for Infrastructure: Uncertainty and Risk. In: Stewart MG, Rosowsky DV, editors. Engineering for Extremes. Springer Tracts in Civil Engineering. Cham: Springer; 2022.
[43] Stewart MG, Ryan PC, Henderson DJ, Ginger JD. Fragility analysis of roof damage to industrial buildings subject to extreme wind loading in non-cyclonic regions. Eng Struct 2016;128:333–43.
[44] Stramit (2012). Stramit purlins, girts and bridging. Stramit Corporation, Australia.
[45] Tomiczek T, Kennedy A, Zhang Y, Owensby M, Hope ME, Lin N, et al. Hurricane damage classification methodology and fragility functions derived from Hurricane Sandy's effects in coastal New Jersey. J Waterw, Port, Coast, Ocean Eng 2017;143 (5):04017027.
[46] USACE (2006). Depth-Damage Relationships for Structures, Contents, and Vehicles and Content-to-Structure Value Ratios (CSVR) in Support of the Donaldsonville to the Gulf, Louisiana, Feasibility Study. US Army Corps of Engineers, LA, USA.
[47] Woolcock, S.T., Kitipornchai, S., Bradford, M.A. and Haddad, G.A. (2011). Design of Portal Frame Buildings. 4th edition. Australian Steel Institute, Sydney, Australia.
[48] Xian S, Lin N, Hatzikyriakou A. Storm surge damage to residential areas: a quantitative analysis for Hurricane Sandy in comparison with FEMA flood map. Nat Hazards 2015;79(3):1867–88.